The Present-Day Simulation and Twenty-First-Century Projection of the Climatology of Extratropical Transition in the North Atlantic

MAOFENG LIU

Department of Civil and Environmental Engineering, Princeton University, Princeton, New Jersey

GABRIEL A. VECCHI

Geophysical Fluid Dynamics Laboratory, National Oceanic and Atmospheric Administration, and Atmospheric and Oceanic Sciences Program, Princeton University, Princeton, New Jersey

JAMES A. SMITH

Department of Civil and Environmental Engineering, Princeton University, Princeton, New Jersey

HIROYUKI MURAKAMI

Geophysical Fluid Dynamics Laboratory, National Oceanic and Atmospheric Administration, and Atmospheric and Oceanic Sciences Program, Princeton University, Princeton, New Jersey

(Manuscript received 2 May 2016, in final form 10 December 2016)

ABSTRACT

This study explores the simulations and twenty-first-century projections of extratropical transition (ET) of tropical cyclones (TCs) in the North Atlantic, with a newly developed global climate model: the Forecast-Oriented Low Ocean Resolution (FLOR) version of the Geophysical Fluid Dynamics Laboratory (GFDL) Coupled Model version 2.5 (CM2.5). FLOR exhibits good skill in simulating present-day ET properties (e.g., cyclone phase space parameters). A version of FLOR in which sea surface temperature (SST) biases are artificially corrected through flux-adjustment (FLOR-FA) shows much improved simulation of ET activity (e.g., annual ET number). This result is largely attributable to better simulation of basinwide TC activity, which is strongly dependent on larger-scale climate simulation. FLOR-FA is also used to explore changes of ET activity in the twenty-first century under the representative concentration pathway (RCP) 4.5 scenario. A contrasting pattern is found in which regional TC density increases in the eastern North Atlantic and decreases in the western North Atlantic, probably due to changes in the TC genesis location. The increasing TC frequency in the eastern Atlantic is dominated by increased ET cases. The increased density of TCs undergoing ET in the eastern subtropics of the Atlantic shows two propagation paths: one moves northwest toward the northeast coast of the United States and the other moves northeast toward western Europe, implying increased TC-related risks in these regions. A more TC-favorable future climate, evident in the projected changes of SST and vertical wind shear, is hypothesized to favor the increased ET occurrence in the eastern North Atlantic.

1. Introduction

Tropical cyclones (TCs) moving poleward can lose their tropical characteristics and evolve into extratropical storm systems through interaction with baroclinic environments in midlatitudes (Jones et al. 2003), a process generally referred to as extratropical transition (ET). The potential hazards from extratropically transitioning TCs include heavy rainfall and expanded gale-force wind (Jones et al. 2003). Tropical Storm Agnes in 1972 (DiMego and Bosart 1982a,b), Hurricane Floyd in 1999 (Atallah and Bosart 2003; Colle 2003), and Hurricane Irene in 2011 (Liu and Smith 2016), for example, produced extreme rainfall and severe flooding in the northeastern United States. All three produced heavy rainfall with a left-of-track concentration of rain at far range from the storm circulation (Atallah and Bosart

Corresponding author e-mail: Maofeng Liu, maofeng@princeton.edu

DOI: 10.1175/JCLI-D-16-0352.1

2003; Colle 2003; Atallah et al. 2007). More recently, Hurricane Sandy in 2012 produced catastrophic storm surge over the coast of the northeastern United States, especially over New Jersey and New York City. The intensification of Sandy was closely associated with ET (Galarneau et al. 2013). Case studies of historical ET storms that have reached Europe highlight their damages through both direct impacts (Thorncroft and Jones 2000; Agustí-Panareda et al. 2005; Feser et al. 2015) and remote impacts (Grams and Blumer 2015). Hurricane Gonzalo (2014) moved from the northern part of the United Kingdom to the Balkans for several days as an extratropically transitioned cyclone and produced strong wind and heavy rainfall, which led to fatalities and economic losses (Feser et al. 2015). Grams and Blumer (2015) found that ET of Hurricane Katia (2011) was responsible for the development of a downstream trough that triggered severe thunderstorms in central Europe.

The potential hazards associated with ET highlight the importance of understanding ET events. Previous studies have focused on the dynamic and thermodynamic evolution of ET events (e.g., Harr and Elsberry 2000; Klein et al. 2000; Jones et al. 2003; Arnott et al. 2004; Davis et al. 2008; Kitabatake 2008; Galarneau et al. 2013). The interaction of TCs with midlatitude troughs plays a crucial role in determining the post-transition intensity and structure of the storm systems (e.g., Harr and Elsberry 2000; Hanley et al. 2001; Klein et al. 2002; McTaggart-Cowan et al. 2003; Ritchie and Elsberry 2003; Hart et al. 2006; Galarneau et al. 2013; Leroux et al. 2013; Griffin and Bosart 2014).

In addition to these studies, there has been research investigating the climatological properties of ET over different oceans. Hart and Evans (2001) examined the ET climatology in the North Atlantic (NA), and found that 46% of TCs experienced ET during the period 1950–99. There is a pronounced seasonal cycle associated with ET in the NA. The latitude with the highest frequency of ET ranges from 35° to 45° (Hart and Evans 2001). A slightly lower ET ratio (40%) was found in the western North Pacific (WNP) during the period 1979–2004 (Kitabatake 2011). An even smaller percentage (only 9%) of TCs in the eastern North Pacific (ENP) undergo ET (Wood and Ritchie 2014). The westward extension of the deep subtropical high from North America to the ENP is suggested to be the main reason of the decreased ET ratio from the NA and the WNP to the ENP (Wood and Ritchie 2014). Increasing trends of ET frequency and ratio were found in both the Northern and Southern Hemispheres over the period of 1970–2012, although there were differences in the magnitude of trends and statistical significances across basins (Mokhov et al. 2014).

Crucial questions left unanswered by the above studies concern the potential role of projected multidecadal climate change on the number and intensity of ET events. High-resolution climate models provide a framework for simulating, predicting and projecting TC activity (e.g., Zhao et al. 2009; Murakami and Wang 2010; Murakami et al. 2012; Chen and Lin 2013; Vecchi et al. 2014; Murakami et al. 2015; Walsh et al. 2015). Studies using climate models found that ET was a key element of a projected increase in storms impacting western Europe under global warming (Haarsma et al. 2013; Baatsen et al. 2015). Studies on future ET activity in the NA, however, remain sparse. This paper aims to provide a comprehensive study on the simulation and projection of ET activity in the NA using a global high-resolution coupled climate model. The significance of this basin is highlighted by the dense population and the economic importance in the northeast coast of the United States and western Europe. High-quality best-track data available in this basin allow a detailed validation of the climate model simulation.

As a first step, we examine the capability of our model in simulating the present-day climatology of ET. Then we use the model to simulate the response of ET under warming scenarios. The paper is organized as follows. In section 2, we introduce data and methods used in this study. Results are presented in section 3, and a summary and conclusions are given in section 4.

2. Data and methods

a. Data

In this study, we use the Atlantic Hurricane Database (HURDAT) best-track data (6-h interval) from National Oceanic and Atmospheric Administration (NOAA)'s National Hurricane Center (NHC). To match the tracking scheme used in the climate model (Murakami et al. 2015; Harris et al. 2016), only TCs with 3-day duration and tropical storm intensity, or greater, are used. HURDAT best-track data provide the timing when a TC changes into an extratropical cyclone (EX) (McAdie et al. 2009). An EX in HURDAT is defined as a system whose major energy source is baroclinic (McAdie et al. 2009). Despite this rather subjective definition, the ET information from HURDAT is compared with climate model results.

Two reanalysis datasets are used in this study: the 6-h National Centers for Environmental Prediction (NCEP) Climate Forecast System Reanalysis (CFSR; Saha et al. 2010) at 0.5° horizontal resolution and the 6-h, 1.25° Japanese 55-Year Reanalysis (JRA-55; Kobayashi et al. 2015). The CFSR and JRA-25 (an earlier version of JRA-55) reanalysis fields have been shown to have the lowest TC position differences from best-track data compared to European Centre for Medium-Range

Weather Forecasts (ECMWF) 40-Year Re-Analysis (ERA-40), ECMWF interim reanalysis (ERA-Interim, hereafter ERA-I), and Modern-Era Retrospective Analysis for Research and Applications (MERRA) (Schenkel and Hart 2012). Murakami (2014) found that JRA-55 and CFSR showed the highest detection rate in terms of hitting rate and false alarm rate compared to other reanalysis datasets. The two datasets are separately combined with the HURDAT best-track data to build the present-day ET climatology over 1979–2005. We use 1979 as the starting year because it is the year CFSR began to provide data, and because NHC started to use satellite information for TC and ET detection operationally since 1970s (McAdie et al. 2009). The ending year is set as 2005 to be consistent with the warming scenario used in our climate simulations, as will be introduced in the following section.

b. *FLOR climate model*

A newly developed Geophysical Fluid Dynamics Laboratory (GFDL) global coupled model, the Forecast-Oriented Low Ocean Resolution (FLOR) model, is employed in this study (Jia et al. 2015; Vecchi et al. 2014). FLOR is a global climate model with high-resolution land and atmosphere components at ~50 km taken from the Coupled Model version 2.5 (CM2.5; Delworth et al. 2012) and low-resolution ocean and sea ice components at ~100 km from the Coupled Model version 2.1 (CM2.1; Delworth et al. 2006; Gnanadesikan et al. 2006; Wittenberg et al. 2006). This coupling method allows us to explore regional-scale extremes at relatively low costs (Vecchi et al. 2014). We use 6-hourly and monthly model outputs in this study. A flux-adjusted version of FLOR (FLOR-FA; Vecchi et al. 2014; Krishnamurthy et al. 2015) is also used. In FLOR-FA, a prescribed climatological adjustment to the SST tendency is applied in order to reduce climatological SST biases. Through the use of climatological adjustment of momentum, freshwater, and enthalpy fluxes between atmosphere and ocean, FLOR-FA aims to provide improved simulations of large-scale climate conditions such as SST and surface wind stress. FLOR-FA exhibits improved skill in simulating the TC climatology and predicting regional TC activity (Vecchi et al. 2014). Whether the improved simulation of TC activity in FLOR-FA will also be seen in ET activity is one of the questions we will address in this study. A detailed description of FLOR and its flux-adjusted version can be found in Vecchi et al. (2014) and Jia et al. (2015).

Historical anthropogenic forcings for aerosols and forcings for volcanic events are prescribed in the FLOR simulations for the period 1861–2005. The representative concentration pathway (RCP) 4.5 scenario is used over 2006–2100 for simulations of the future climate. To evaluate the changes of ET activity, we explore five ensembles over two simulation periods: the present-day (PD) run over 1961–2005, and the global warming (GW) run over the last 45 years (2056–2100) of the twenty-first century as we expect to cover the ending year of the simulation.

The tracking scheme applied here is the same as the one developed by Harris et al. (2016) and implemented by Murakami et al. (2015). Based on 6-hourly snapshots of atmospheric conditions, TCs are tracked mainly using minimum sea level pressure and temperature anomaly between 300 and 500 hPa (Murakami et al. 2015). To represent regional TC activity, we define the annual track density of each grid cell (1°) as the total number of days in a year for which the center of circulation of a TC is within 500 km of the grid (Vecchi et al. 2014). The use of a 500-km radius agrees with the typical TC size used in ET studies (Evans and Hart 2003; Hart 2003) and is consistent with observational studies (e.g., Chavas and Emanuel 2010). In this study, TC genesis is defined as the starting point of each TC detected by the tracking scheme.

c. *Cyclone phase space*

There have been studies using different dynamical or thermodynamical variables to define the time for ET onset and/or completion, such as warm frontogenesis (Harr and Elsberry 2000), thickness asymmetry and thermal wind in cyclone phase space (CPS) (Evans and Hart 2003; Hart 2003), 500-hPa geopotential height open wave (Demirci et al. 2007), and isentropic potential vorticity (Kofron et al. 2010b). It has been found that the open-wave and frontogenesis approaches fail to distinguish ET and recurving non-ET events (Kofron et al. 2010a) and cannot provide consistent results for the completion time using different data sources as inputs (Wang et al. 2012). The CPS method is the only approach that has objective definitions of ET onset and completion time. It has been widely used for case studies (Arnott et al. 2004; Hart et al. 2006; Griffin and Bosart 2014) and ET climatology studies in the WNP (Kitabatake 2011; Song et al. 2011) and ENP (Wood and Ritchie 2014). CPS only requires geopotential heights at isobaric levels as inputs and thus can be easily applied to climate model results. It is used here to discriminate ET and non-ET events and also to determine the ET onset and completion time.

In CPS, the 900–600-hPa geopotential thickness asymmetry (B), low-level (900–600 hPa) thermal wind ($-V_T^L$), and upper-level (600–300 hPa) thermal wind ($-V_T^U$), are used to describe evolving thermal characteristics of a TC. High values of B imply frontal systems while values close to 0 reflect thermally symmetric systems (in this case a TC). Positive thermal wind values

TABLE 1. Evaluation statistics of simplified cyclone phase space (CPS) results vs standard CPS outputs over 1979–2005 with CFSR. Probability of detection (POD) is defined as $H(H+M)^{-1}$ and false alarm ration (FAR) as $F(H+F)^{-1}$, where H is an ET event detected by standard CPS and detected by simplified CPS, M is an ET event detected by standard CPS but not detected by simplified CPS, and F is an ET event not detected by standard CPS but detected by simplified CPS. Bias (h) and root-mean-square error (RMSE; h) are presented for ET onset time (B), ET completion time (E), and ET time duration (D).

POD	FAR	$BIAS_B$	$RMSE_B$	$BIAS_E$	$RMSE_E$	$BIAS_D$	$RMSE_D$
0.96	0.08	−7.68	21.82	−7.65	21.68	0.02	13.21

indicate warm-core systems while negative thermal wind values indicate cold-core systems. Detailed descriptions of the three parameters are found in Evans and Hart (2003) and Hart (2003). Evans and Hart (2003) defined the onset of ET at the time that B exceeds 10 m and the completion at the time that $-V_T^L$ becomes negative. This definition does not capture all TCs since there are cases in which TCs become cold-core systems before they gain asymmetric characteristics. This is found in 16.8% of all ET events over the WNP (Kitabatake 2011) and most cases over the ENP where the rather low SST may play a large role (Wood and Ritchie 2014). In our study, the first time B exceeds 10 m or $-V_T^L$ becomes negative is set as the onset of ET. The first time B exceeds 10 m and $-V_T^L$ becomes negative is defined as the completion of ET.

In the standard CPS method, thermal winds are computed through linear regression of geopotential heights at multiple isobaric levels. Because of the limitation of storage space, 6-hourly geopotential heights from FLOR model outputs are only available at three isobaric levels. Therefore, we form a simplified version of the CPS method. The term B is calculated as the thermal thickness difference between 850 and 500 hPa. The terms $-V_T^L$ and $-V_T^U$ are based on 850–500-hPa and 500–300-hPa height fields, respectively. The suitability of the simplified CPS method is compared against the standard algorithm in section 3a.

3. Results

a. Present-day CPS and ET climatology

We start by comparing the simplified CPS method to the standard CPS for the period 1979–2005 with CFSR data as inputs (Table 1). The simplified CPS exhibits good skill in detecting ET events with a probability of detection (POD) reaching 0.96 and false alarm ratio (FAR) of 0.08. For reference a perfect match is achieved when POD reaches 1 and FAR is 0. The mean biases and root-mean-square errors of ET onset and completion time are less than 8 and 22 h, respectively. Given that the temporal resolution is 6 h, these results indicate that simplified CPS matches well with standard CPS. We further examine the capability of the simplified CPS in simulating the temporal evolution of ET using four hurricanes as examples (Fig. 1). The four hurricanes represent different development paths on the CPS diagram. Three of the four TCs (all except Rita) experienced ET. The simplified CPS method accurately captures the evolution of these four TCs in terms of the B versus $-V_T^L$ diagram (Fig. 1). These results give us confidence in using the simplified CPS to study ET climatology.

A good representation of CPS climatology is a prerequisite for analyzing model-simulated ET climatology. Both FLOR and FLOR-FA capture the general spatial pattern of the frequency map of B versus $-V_T^L$ as compared to reanalysis datasets (Fig. 2). Our models and reanalysis fields agree that symmetric and warm-core storms have the highest frequency among all phases. They also agree that more thermally asymmetric storms tend to have higher strength cold cores. FLOR-FA and CFSR have larger ranges of $-V_T^L$ (i.e., higher strength of warm cores) than JRA-55, which may be partly attributed to the finer spatial resolution. Another reason may be the underestimation of TC intensity in JRA-55 due to errors in wind profile retrievals. Note that in JRA-55 wind profiles are estimated from the climatological relation between the maximum wind and the wind radius when the radius of 30- and 50-kt wind is not available in the best-track data (Hatsushika et al. 2006), which may artificially produce weaker TCs.

The CPS frequency diagram of $-V_T^L$ versus $-V_T^U$ is presented in Fig. 3. Like the B versus $-V_T^L$ diagram, FLOR-FA and FLOR reproduce the basic patterns obtained from reanalysis fields. The peak frequency from the two reanalysis fields has low-intensity warm-core structures throughout the vertical column of TC vortexes. The peak frequency in FLOR-FA and FLOR is translated slightly toward upper-level cold core structures. It coincides with vortices with low-level warm cores and upper-level cold cores. The bulge in the lower-right region of the frequency diagram for FLOR models shows that there are more TCs with low-level warm cores and high-level cold cores in FLOR simulations than in the two reanalysis datasets.

In addition to the CPS frequency diagram, the spatial pattern of B and $-V_T^L$ provide a way to examine the capability of FLOR to simulate CPS climatology (Figs. 4 and 5, respectively). FLOR models capture the meridional changes of B (Fig. 4). As TCs move northward from the tropics, they gradually gain frontal characteristics as B increases. It appears that 30°N roughly represents the critical latitude that distinguishes between symmetric ($B < 10$ m) and frontal

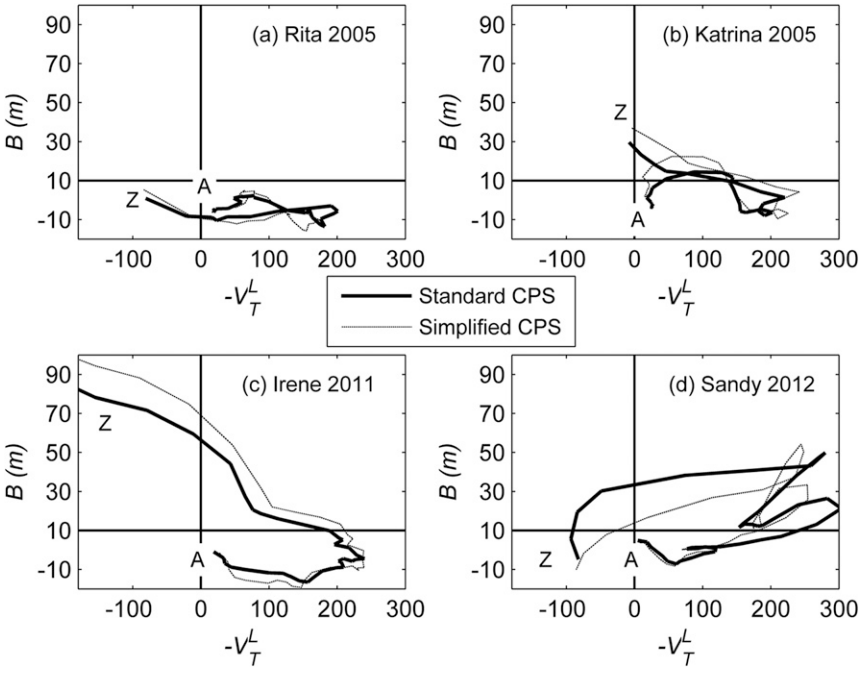

FIG. 1. The cyclone phase space (CPS) diagram of geopotential thickness asymmetry (i.e., B) and 900–600-hPa thermal wind (i.e., $-V_T^L$) from standard and simplified CPS for Hurricanes (a) Rita (2005), (b) Katrina (2005), (c) Irene (2011), and (d) Sandy (2012) using CFSR data as inputs. The letters A and Z indicate the starting and end of the TC life cycle, respectively.

($B > 10$ m) storms. The meridional changes are also found in $-V_T^L$ (Fig. 5). The increasing strengths of TC warm cores can be seen in increases of $-V_T^L$ as TCs move from the deep tropics to subtropics and then to midlatitudes. In midlatitudes between 30° and 40°N, the combination of Figs. 4 and 5 indicates asymmetric TCs with warm core structures. These storms have so-called hybrid structures because they are undergoing ET and have properties of both TCs and EXs (Evans and Hart 2003; Hart et al. 2006). After reaching its peak, $-V_T^L$ shows a gradually decreasing trend as TCs continue to move poleward, suggesting the decaying of warm-core structures. FLOR-FA and CFSR have higher $-V_T^L$ peaks than JRA55. This is consistent with the CPS frequency diagram results (Fig. 2).

We evaluate ET climatology through analyses of basinwide aggregated TC activity in the NA (Table 2), focusing on annual TC counts, ET counts, and ET ratio (i.e., the ratio between ET and TC counts). The standard FLOR model largely underestimates the annual TC counts and simulates around half of the observed TCs. The flux-adjusted version of FLOR model exhibits fewer but comparable annual TC counts compared to HURDAT. The development of the flux adjustment procedure is based on the hypothesis that biases in the large-scale climate conditions constrain the ability of climate models in simulating TC activity (Vecchi et al. 2014). The superiority of FLOR-FA over FLOR in simulating the aggregated TC number implies that TC simulation is markedly improved after flux adjustment. In terms of ET counts and ET ratio, FLOR-FA also provides much better results than FLOR (Table 2), implying that good representations of CPS parameters as shown in Figs. 2–5 are not sufficient to ensure good simulations of ET climatology. All ET ratios for the period 1979–2005 are above 50% except in the FLOR model (30.8%) (Table 2), indicating the impact of SST biases in ET probability.

We now explore the underlying reason for the better performance of FLOR-FA, compared with FLOR, in simulating ET activity. A majority of TC tracks in FLOR are below ~30°N, which is likely due to the model's systematic bias in representing the large-scale TC environment (Fig. 6). More specifically, underestimating SST and overestimating vertical wind shear [Figs. 2 and 3 in Vecchi et al. (2014)] inhibit TC development and northward propagation.

Based on the hypothesis that TCs moving into the baroclinic zone are more likely to undergo ET, Hart and Evans (2001) used the monthly 700-hPa climatological Eady growth rate (Hoskins and Valdes 1990) to represent the baroclinically favorable zone for ET occurrence

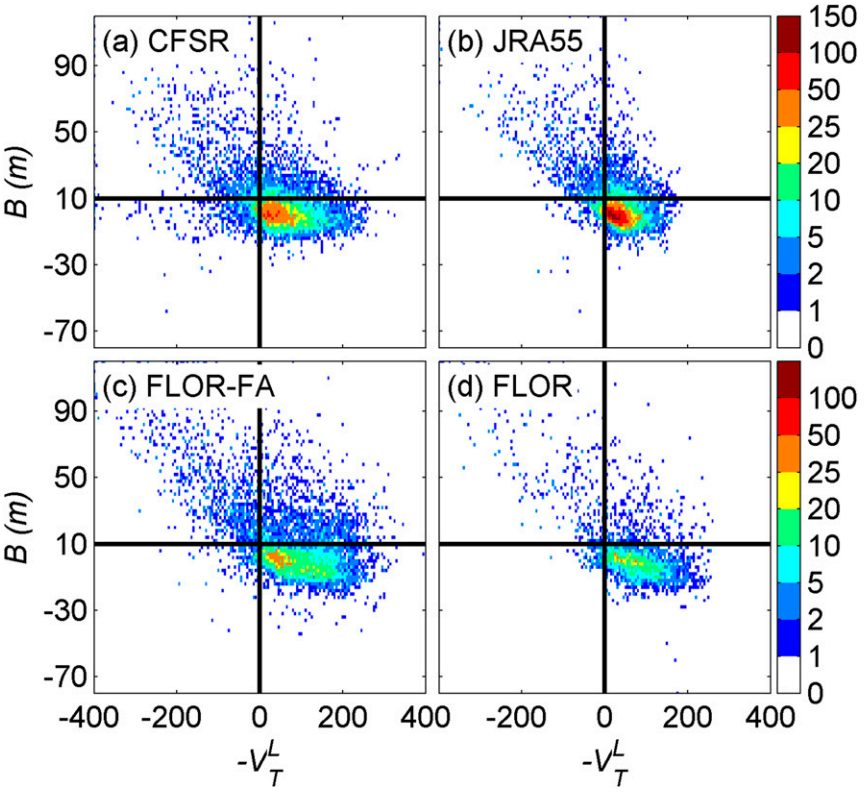

FIG. 2. The CPS frequency of B vs $-V_T^L$ diagram over 1979–2005 from (a) CFSR, (b) JRA-55, (c) FLOR-FA, and (d) FLOR. The first ensemble from FLOR-FA and FLOR simulations is used, respectively. 264 TCs are used for CFSR and JRA55, and 99 and 184 TCs from the first ensemble for FLOR and FLOR-FA, respectively.

and then explained the seasonal cycle of ET activity in the NA. The Eady growth rate is defined by

$$\sigma = 0.31 f \frac{dU}{dz} N^{-1}, \tag{1}$$

where f is the Coriolis parameter, dU/dz is the monthly 850–250-hPa vertical wind shear, and N is the 700-hPa monthly Brunt–Väisälä frequency. Note that monthly geopotential heights are available at denser levels, which allows us to compute 850–250-hPa wind shear. We use a threshold of $\sigma = 0.25\,\text{day}^{-1}$, like Hart and Evans (2001) and Kitabatake (2011), for distinguishing environments favorable for ET; values below $0.25\,\text{day}^{-1}$ are unfavorable for baroclinic development. Fewer TCs in FLOR reach the baroclinic zone than in HURDAT and FLOR-FA (Fig. 6), resulting in a lower number of TCs undergoing ET. Given the inability of the standard FLOR model in simulating basinwide ET activity, we will focus on FLOR-FA in subsequent analyses.

ET and non-ET events show distinct track characteristics. The capability of FLOR-FA and CPS methods in capturing their differences is a key for assessing ET climatology. The TC density maps for ET and non-ET events from FLOR-FA are compared with those from reanalysis and HURDAT, respectively (Fig. 7). Note that classification of ET and non-ET events in HURDAT does not rely on the CPS method. JRA-55 and CFSR results resemble the spatial distribution of TC density of ET/non-ET cases in HURDAT (Figs. 7a–c,e–g), suggesting good skill of CPS in distinguishing the ET and non-ET cases. FLOR-FA captures many key features of the density of ET/non-ET storms (Figs. 7d,h): 1) the tracks of non-ET cases are generally constrained below ~40°N, implying less impact in midlatitudes than ET events; 2) non-ET storms show relatively high occurrences in the Gulf of Mexico, suggesting that this area may not provide a favorable environment for ET development; and 3) TCs undergoing ET can pass through the midlatitudes toward high latitudes. A possible reason for 2) is that northward tracking TCs may lose the energy source from warm seawater after making landfall in the north of the Gulf of Mexico, and decay before starting ET (Hart and Evans 2001).

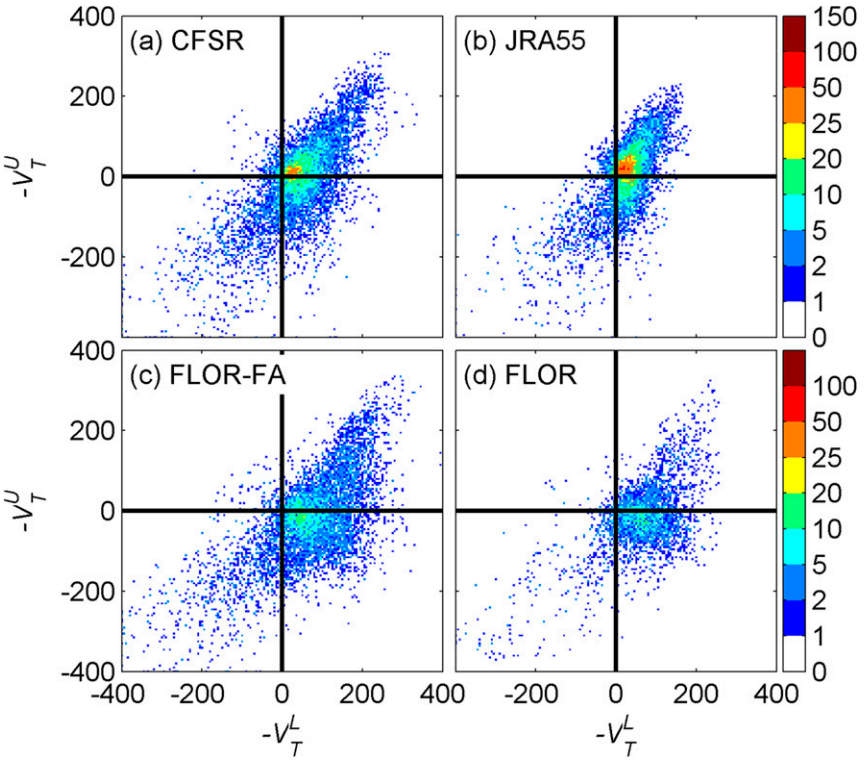

FIG. 3. As in Fig. 2, but for the CPS frequency of $-V_T^L$ vs $-V_T^U$ diagram.

ET is often characterized by interactions between the TC and a pre-existing midlatitude trough (e.g., Harr and Elsberry 2000; Klein et al. 2000; Hanley et al. 2001; Jones et al. 2003; Arnott et al. 2004; Hart et al. 2006). The dynamic evolution of the ET process is highlighted in storm-centered geopotential height composites using all ET events from FLOR-FA (Fig. 8). We focus on the beginning (labeled T_B) and end (labeled T_E) of ET and two other timings, that is, $T_B - 24$ h and $T_E + 24$ h. The results are broadly consistent with 500-hPa geopotential height analyses in Hart et al. (2006) and analyses using CFSR (figures not shown). At the 850-hPa level, the TC composite is embedded in a nearly barotropic environment and shows a prominent vortex 24 h before ET (Fig. 8i). The strong ridge to the east of the TC composite highlights the role of the North Atlantic subtropical high. TCs move northward over time and pass around the ridge (Figs. 8i–l). As ET begins, TCs experience an increasingly baroclinic environment highlighted by tightened geopotential heights (Fig. 8j). During ET, the inner vortex of TC composites gradually decays over time (Figs. 8j–l) (Jones et al. 2003). A loosely organized vortex embedded in a strong baroclinic environment is then observed 24 h after ET. The 500- and 300-hPa geopotential heights reveal the interaction between the TC composite and the midlatitude upper-level trough (Figs. 8a–h). As the TC composite moves closer to the trough, it gradually loses the strength of the vortex (shown in the 500-hPa geopotential height) and is merged into the baroclinic environment once ET completes (Figs. 8e–h).

The change of rainfall distribution during ET is an important element of model evaluation. A TC typically produces rainfall with a symmetric distribution relative to its storm center. As ET occurs, the spatial distribution of TC rainfall develops an increasingly asymmetric pattern with maximum rainfall to the left (right) of the storm center in the Northern (Southern) Hemisphere (e.g., Atallah and Bosart 2003; Colle 2003; Jones et al. 2003; Atallah et al. 2007; Chen 2011). The ability of FLOR-FA to capture changing rainfall structure as ET proceeds is evaluated through examination of the storm-motion-relative 6-h rainfall composites (Fig. 9). In the TC stage, the rainfall field shows a near-symmetric distribution with decreasing rain rate from storm center (Fig. 9a). The maximum rainfall is shifted slightly right of the circulation center, consistent with observations [see Fig. 1a in Villarini et al. (2014)]. The periods in which TCs undergo ET or evolve into EXs are referred to as the ET/EX stage. The composite rainfall in this stage is concentrated in the front-left quadrant of the storm center with back quadrants producing negligible

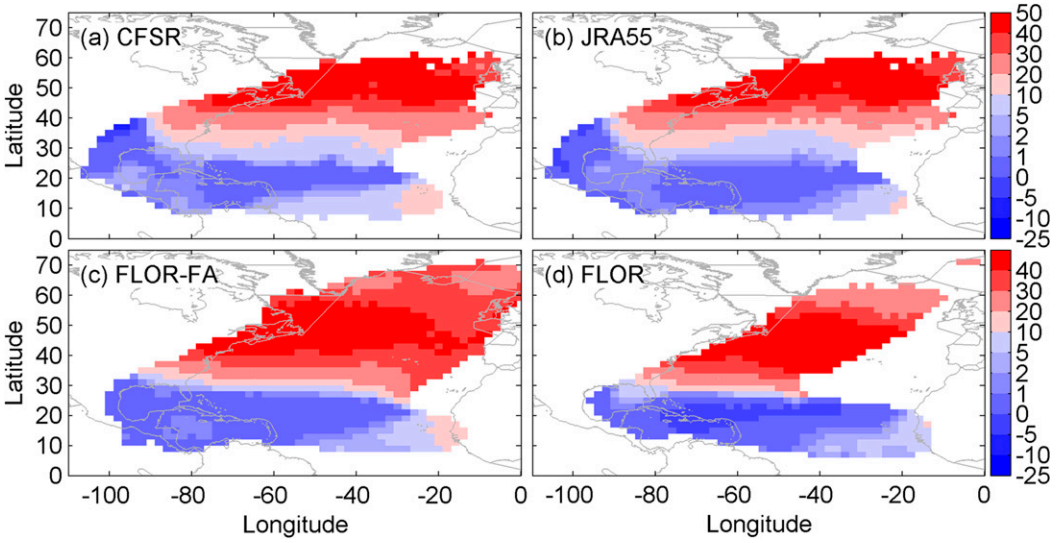

FIG. 4. The mean spatial pattern of B (m) over 1979–2005 from (a) CFSR, (b) JRA-55, (c) FLOR-FA, and (d) FLOR; B is not shown in areas with annual TC density lower than 0.25 TC days. 264 TCs are used for CFSR and JRA-55, and 589 and 983 TCs from all five ensembles for FLOR and FLOR-FA, respectively. The same TC numbers are used for figures hereafter.

rainfall (Fig. 9b), consistent with previous results (e.g., Atallah et al. 2007). The capability of FLOR-FA to capture the rainfall distribution during ET highlights its skill in simulating synoptic-scale ascent in the front-left region of TCs caused by the interactions with mid-latitude troughs to the northwest of TCs (Fig. 8) (Harr and Elsberry 2000; Atallah and Bosart 2003; Jones et al. 2003; Atallah et al. 2007).

The examination of the latitude at which ET begins and completes (Fig. 10) highlights the ability of the FLOR model to simulate the baroclinic features of the TC environment. Compared to CFSR and JRA-55, FLOR-FA exhibits good skill in capturing the latitude distribution of ET onset with mean latitude around 35°N (Fig. 10a), broadly consistent with the critical latitude line between symmetric and asymmetric TCs shown in Fig. 4. The latitudinal distribution of ET completions from FLOR-FA compares well with results from HURDAT and from reanalysis data (Fig. 10b). Previous studies showed that the ET location has a higher frequency in the range of 35°

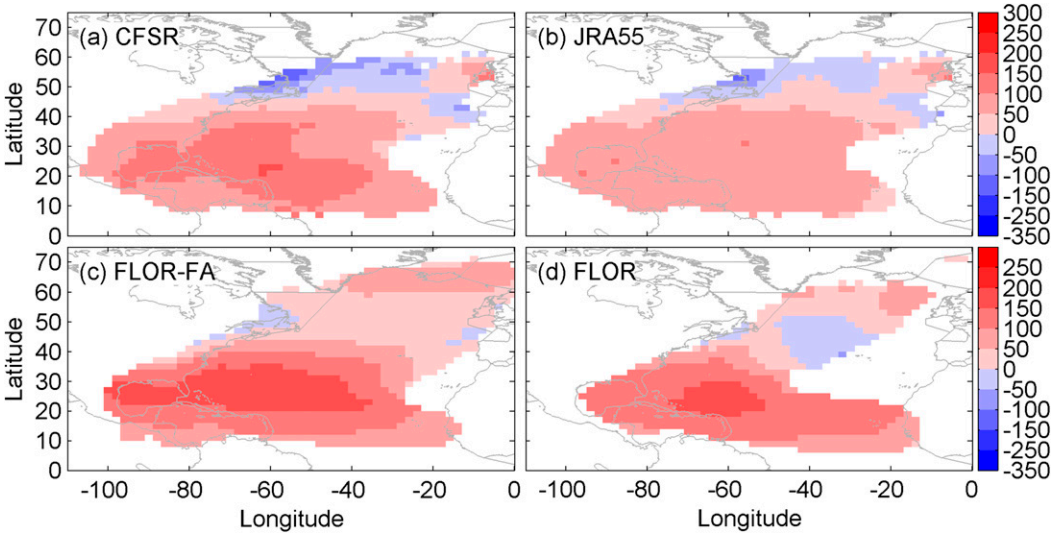

FIG. 5. As in Fig. 4, but for $-V_T^L$.

TABLE 2. Annual TC and ET counts and ET ratio (%) from reanalysis and FLOR models over 1979–2005. In the FLOR-FA and FLOR columns the numbers following '±' are one standard deviation from five ensemble simulations of FLOR models.

	HURDAT	CFSR	JRA-55	FLOR-FA	FLOR
TC No.	9.8	9.8	9.8	7.3 ± 0.5	4.4 ± 0.8
ET No.	5.0	5.5	4.9	4.2 ± 0.4	1.3 ± 0.3
ET ratio (%)	51.1	56.4	50.4	57.3 ± 3	30.8 ± 3

to 45°N over 1899–1996 (Hart and Evans 2001), which is well within the range of 25th and 75th percentiles in FLOR-FA. The 25th and 75th percentiles and mean value in FLOR-FA show closer agreement with HURDAT than the two reanalysis datasets (Fig. 10b). FLOR-FA covers a larger latitude range for ET completion than the other three (e.g., the 90th percentile reaches around 60°N), which may be partly attributable to larger samples for the FLOR-FA results, and partly due to the slight overestimation of warm-core intensity in terms of $-V_T^L$ in midlatitudes (Fig. 5).

The spatial distribution of transition locations is well represented in FLOR-FA compared to reanalysis results (Fig. 11). The transition locations show a southwest–northeast orientation and move toward northeast from ET onset to completion. FLOR-FA misses some details of ET initiation and completion, including underestimation of transition density that occurs inland and overestimation of transition density over regions between Canada and western Europe. The overestimation may be attributable to the overestimation of warm core intensity (Fig. 5) in the FLOR-FA simulation. The simulated TCs with higher strength warm cores may need to propagate to higher latitudes before they become cold core systems.

In this section, we have evaluated several key aspects of CPS and ET climatology. Although FLOR exhibits good skill in simulating present-day ET properties (e.g., CPS parameters), FLOR-FA shows much better simulation of ET activity (e.g., ET ratio) due to its better representation of large-scale environmental conditions affecting TC activity in tropical and subtropical regions. In the next section we will focus on the changes of ET under global warming using FLOR-FA.

b. *Projected changes of ET activity*

As shown in Fig. 12, the annual TC number in the NA shows little change (no statistical significance found, $p = 0.40$). The sign and range of TC frequency changes in the NA under future climate scenarios remain an active area of research (e.g., Knutson et al. 2008; Vecchi et al. 2008; Villarini and Vecchi 2012; Camargo 2013; Emanuel 2013; Knutson et al. 2013). The Intergovernmental Panel on Climate Change (IPCC)

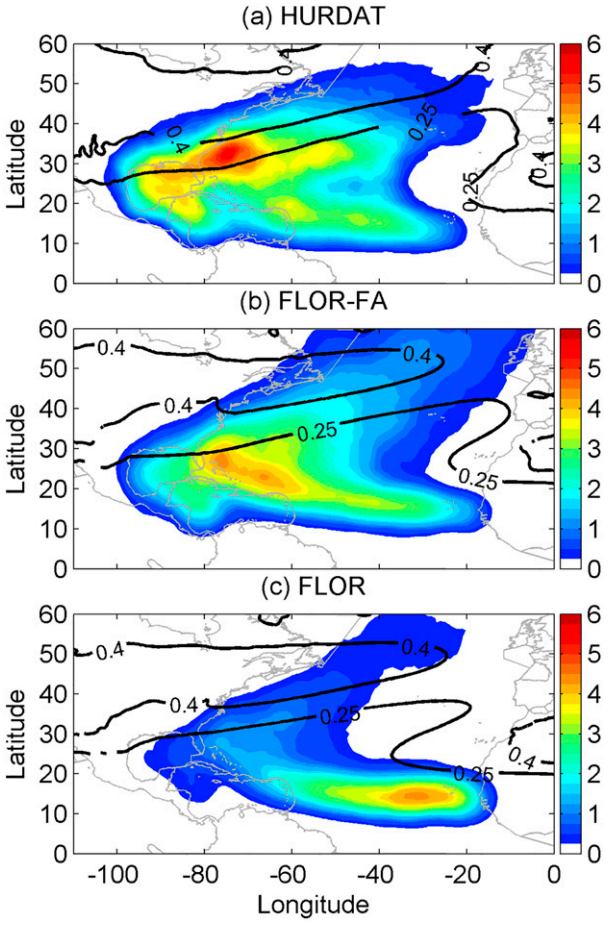

FIG. 6. The annual TC density (shaded) in terms of TC days averaged over 1979–2005 for (a) HURDAT, (b) FLOR-FA, and (c) FLOR. The 700-hPa climatological Eady growth rate (black contours; day^{-1}) from each dataset is also presented.

Fifth Assessment Report (IPCC 2013) presented a wide range of projected future changes in TC frequency in the NA [see Fig. 14.17 in IPCC (2013)]. A further exploration of basinwide TC occurrence changes is beyond the scope of this study. Despite the absence of statistical significance ($p = 0.19$), annual ET counts, unlike TC frequency, show an increasing trend. The increasing annual ET ratio, with a significance level of 0.06, implies that the probability for a TC to undergo ET increases.

Because of regional variability of TC and ET activity, exploring the spatial distribution of TC and ET events may be more valuable than basin-aggregated TC and ET counts since it provides information on regional TC activity, including landfalling TCs (e.g., Murakami and Wang 2010; Vecchi et al. 2014; Vecchi and Villarini 2014; Wright et al. 2015). The spatial patterns of TC density under present-day and global warming scenarios and their differences are shown in Fig. 13. From PD to

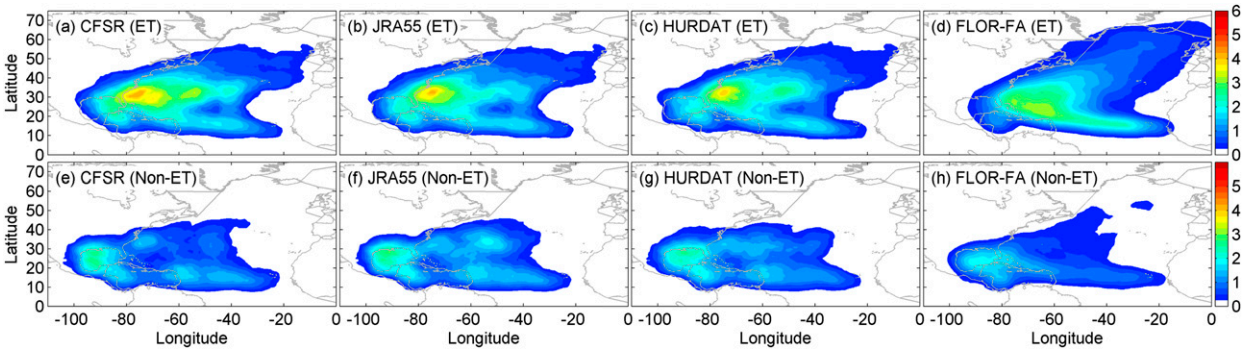

FIG. 7. The annual TC density in terms of TC days averaged over 1979–2005 for (a)–(d) ET events and (e)–(f) non-ET events.

GW, the frequency of TC occurrence shows a substantial decrease over the western NA including the Caribbean Sea, Gulf of Mexico, and southern United States, while a spatially variable increase is found in the tropical eastern NA and northwestern NA (i.e., 37°–42°N, 65°–75°W).

The eastward shift of TC tracks in the NA has been reported in observational studies using TC datasets over the past 120 years (Vecchi and Knutson 2008) and in future projection studies (e.g., Murakami and Wang 2010; Colbert et al. 2013). Murakami and Wang (2010) argued that changes of TC genesis locations are the main

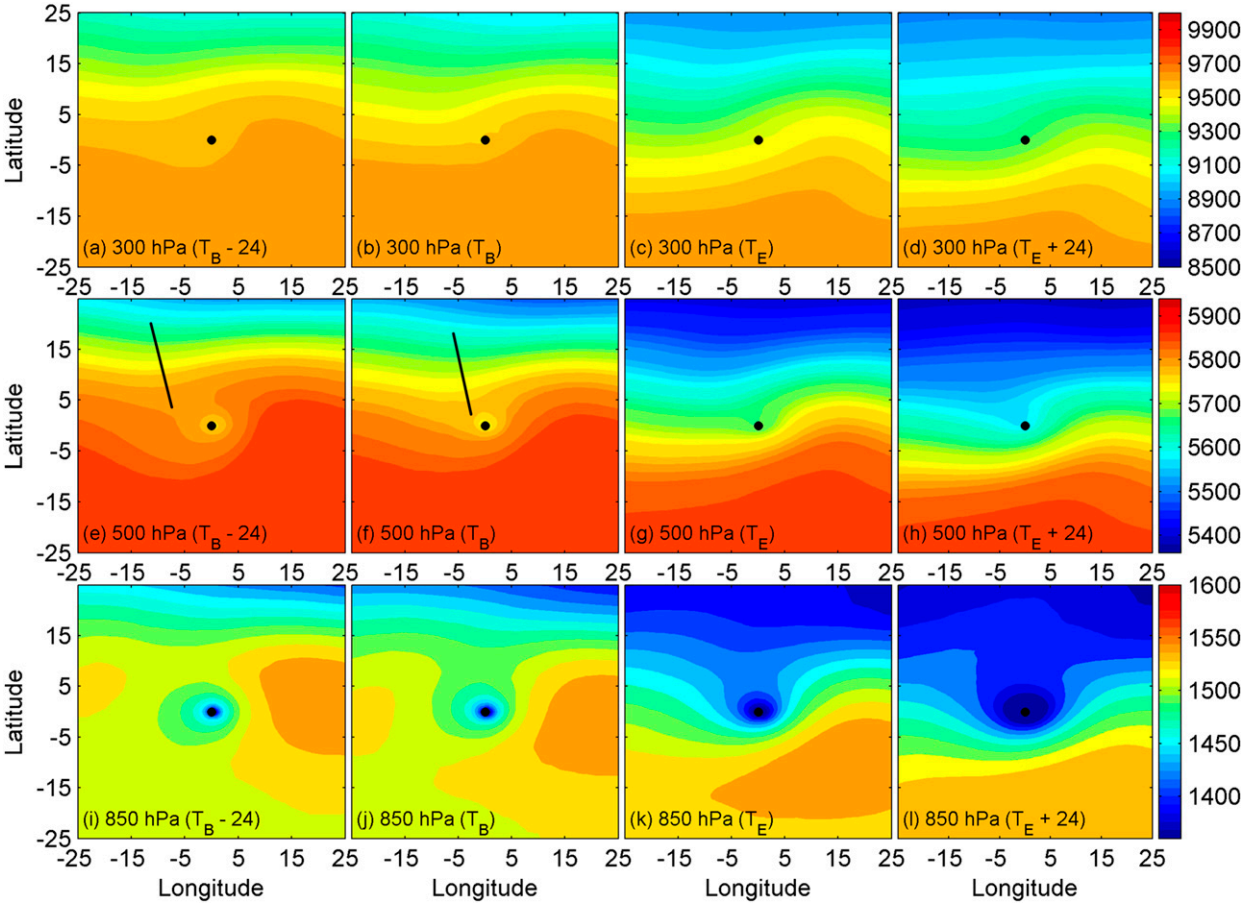

FIG. 8. Storm center-based (a)–(d) 300-, (e)–(h) 500-, and (i)–(l) 850-hPa geopotential height (m) composite from FLOR-FA over 1979–2005. The solid black line indicates the trough axis. The beginning and end time of ET are labeled as T_B and T_E, respectively. The x and y axes are degrees from storm centers. The y axes are in the south–north direction.

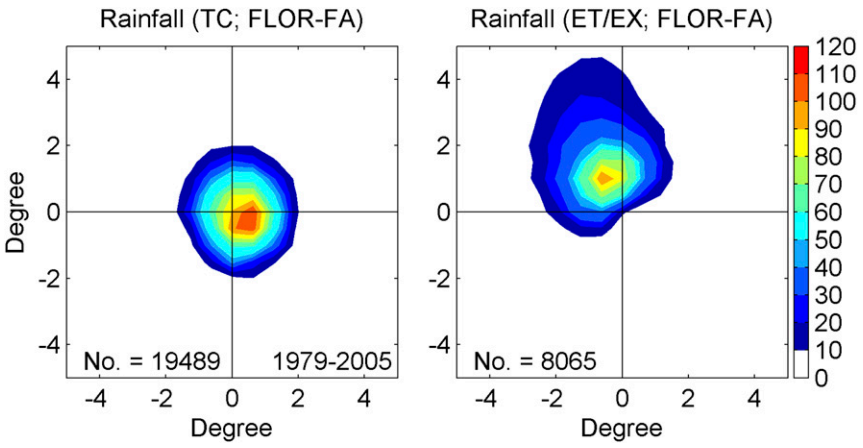

FIG. 9. The storm-motion-relative rainfall composite (mm day^{-1}) from FLOR-FA over 1979–2005: (left) rainfall composite from TCs and (right) rainfall composite from TCs undergoing ET or extratropical cyclones (EX) as identified by CPS. The number of samplings (N) is shown in the bottom left corner.

reason for the shift. TC genesis increases in the eastern NA and decreases in the western NA, causing a shift of tracks from the western to the eastern part of the NA. Colbert et al. (2013) found that the increasing westerly large-scale steering flow is mainly responsible for the shifting of tracks. In this study we explored both TC genesis and large-scale steering flow. The TC genesis exhibits a contrasting pattern between the eastern and western NA, with an increase in the eastern tropics and a decrease in the southern Caribbean Sea (Fig. 14). From the PD to GW run, the ensemble-mean large-scale steering flow shows a slight increase of easterlies from 20° to 30°N, which does not support the eastern shift of TC frequency (figure not shown). Individual ensemble runs do not exhibit consistent changes of the large-scale steering flow. For example, ensemble 1 shows easterlies whereas ensemble 4 exhibits westerlies at 20°–30°N. The results from FLOR-FA are more consistent with the interpretation of Murakami and Wang (2010). Murakami and Wang (2010) found that the increase of TC genesis in the eastern NA is attributable to increased convective available potential energy and background ascent while the decrease of TC genesis in western NA is due to the decrease of midtropospheric humidity and background ascent.

To understand future changes of TC density from ET and non-ET events, we divide all TC events into these two categories using the CPS method (Fig. 15). For both ET and non-ET cases, the occurrence decreases in the western NA (i.e., west of 70°W). The decreases occur, however, in distinct regions, principally the northern Caribbean Sea and the southern United States for ET events and the southern Caribbean Sea and the Gulf of Mexico for non-ET cases (Figs. 15c,f). ET events are more likely to move to higher latitudes than non-ET events, so the decreased density of ET events is found in the northern part of the western NA. Reductions in non-ET cases are found in the lower Caribbean Sea due to constraints of poleward propagation and in the Gulf of Mexico where a relatively high non-ET density is found (Figs. 7e–h).

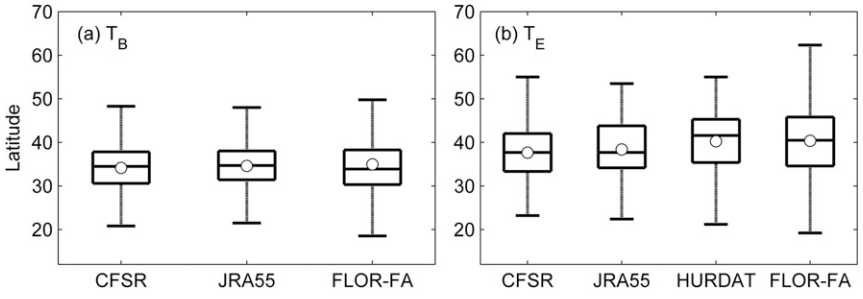

FIG. 10. Box plots of latitude (°) at (a) ET onset and (b) ET completion over 1979–2005. The limits of whiskers represent the 10th and 90th percentiles. The limits of boxes represent the 25th and 75th percentiles. The line inside the boxes and the open circle indicate median and mean, respectively.

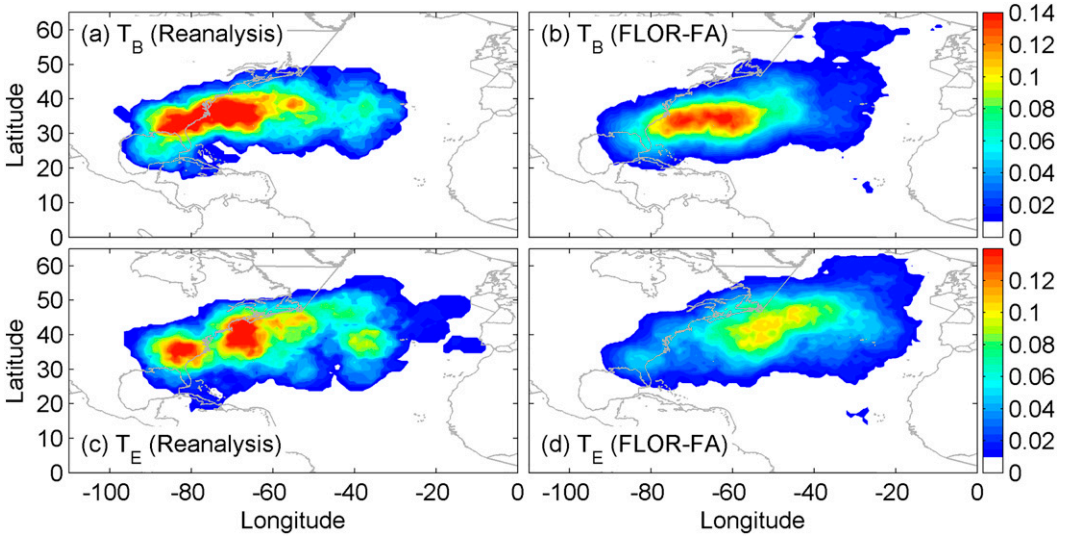

FIG. 11. The TC density at timings of (a),(b) ET onset and (c),(d) ET completion over 1979–2005. In (a) and (c) the TC density of reanalysis is represented by the mean of CFSR and JRA-55.

The increase of future TC occurrence over the tropics and subtropics in the eastern NA (Fig. 13c) is also seen in the annual TC density changes of ET events (Fig. 15c). More interestingly, the increased ET events are concentrated in two clear paths: one moves northwest toward the northeast coast of the United States including New England area, and the other moves northeast toward western Europe (Fig. 15c). The density changes of all TC events show a similar pattern (Fig. 13c) but the paths are somewhat mixed with the density changes in non-ET events (Fig. 15f). The finding that more future TCs reach western Europe is consistent with recent studies by Haarsma et al. (2013) and Baatsen et al. (2015). Haarsma et al. (2013) used an atmospheric climate model (EC-EARTH; Hazeleger et al. 2010) with prescribed SST and found that more hurricanes associated with ET are likely to hit western Europe under global warming scenarios. Baatsen et al. (2015) extended this work with more details of the storm characteristics and found that both frequency and intensity of storms hitting Europe increase in a warming climate. The increased TC activity reaching Europe is dominated by ET events, highlighting the potentially growing threat to Europe (Figs. 15c,f).

Large-scale climate conditions provide important environments for TC genesis and development (e.g., Camargo et al. 2007; Kossin et al. 2010; Murakami and Wang 2010; Villarini et al. 2010; Colbert and Soden 2012; Villarini et al. 2012; Colbert et al. 2013; Murakami et al. 2013; Vecchi et al. 2014). We further explore density changes of ET events by examining changes in the large-scale climate condition under global warming (Fig. 16). Specifically, increased future SST and decreased 850–250-hPa wind shear in the tropics/subtropics highlight an increasingly favorable environment for TC development (Figs. 16c,f). We hypothesize that TCs are more likely to reach midlatitude baroclinic zones in such a more favorable climate. The baroclinic instability represented by 700-hPa monthly Eady growth rate shows little change south of 40°N (Fig. 16f), which in itself does not affect the ET activity. ET occurrences, however, increase with more TCs moving to midlatitudes (Hart and Evans 2001; Kitabatake 2011).

The future TC/ET change can be illustrated using a schematic map (Fig. 17). With lower TC genesis frequency in the western NA under global warming, we observe density decreases of both ET and non-ET

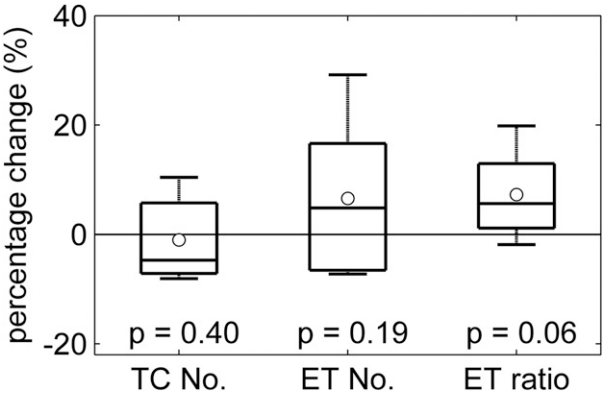

FIG. 12. Future change (%) in annual TC counts, ET counts and ET ratio [i.e., percentage differences between the RCP4.5 (global warming; GW) and present-day (PD) runs]. The p value is calculated using one-sided Mann–Whitney–Wilcoxon tests.

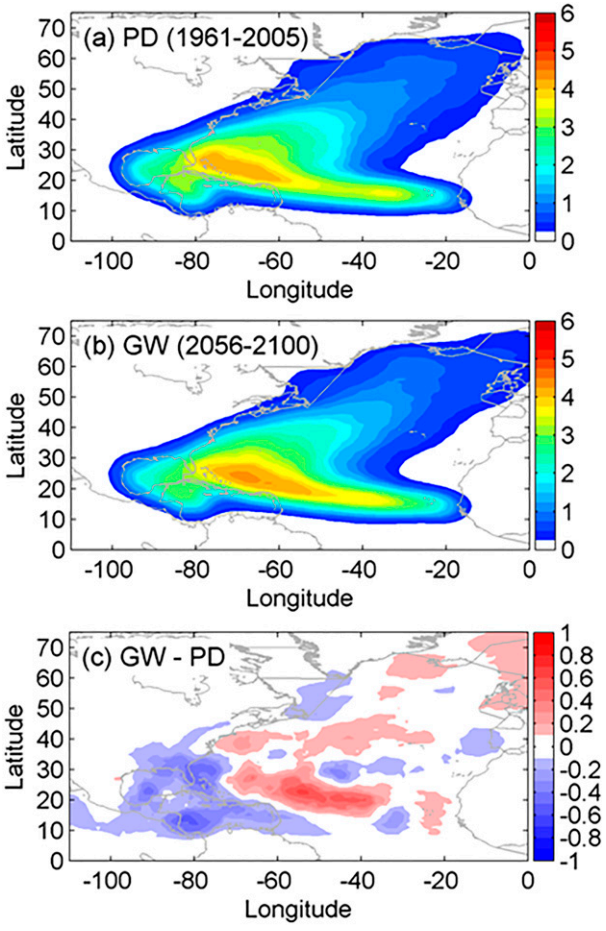

FIG. 13. The annual TC density in the (a) PD and (b) GW simulations. (c) The future change of annual TC density.

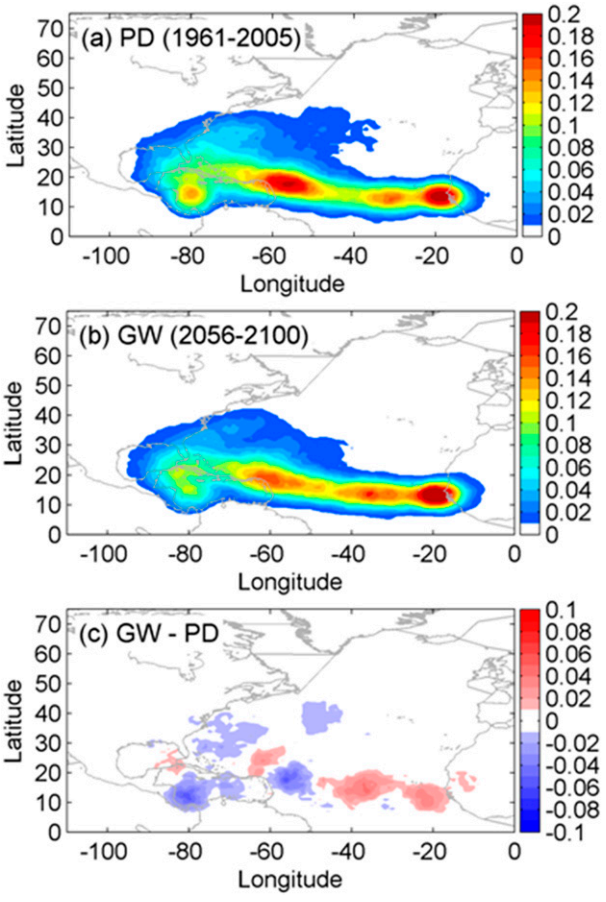

FIG. 14. The annual TC genesis density in the (a) PD and (b) GW simulations. (c) The future change of annual TC genesis density.

activity in that region. The increased TC genesis in the eastern NA enhances the ability of TCs to reach midlatitudes, due to a more favorable TC environment, and thus increases the probability of ET occurrence. ET events dominate the increased future TC density in midlatitudes of the eastern NA along two paths: one reaches the northeastern coast of the United States and the other moves toward western Europe.

4. Summary and conclusions

In this study we examine the capability of the FLOR model to simulate the present-day climatology of ET of TCs in the NA and we present an initial assessment of the potential changes of ET under the RCP4.5 scenario. The CPS method is used to determine the onset and completion time of ET events. Two reanalysis datasets, JRA-55 and CFSR, are used to explore present-day ET climatology and to compare with results from the FLOR models. The principal conclusions are listed below.

The standard and flux-adjusted versions of the FLOR model are able to reproduce important features of the CPS climatology in the NA. Most notably, the model accurately represents the CPS frequency diagram and the spatial pattern of CPS variables, compared to CFSR and JRA-55 analyses.

The FLOR model without flux adjustment simulates fewer ET events and has a smaller annual ET ratio (i.e., the ratio of TCs that undergo ET), compared with analyses based on HURDAT data and reanalysis fields. FLOR-FA exhibits improved skill in simulating annual ET counts and the ET ratio. FLOR underestimates the ET ratio (30.8% ± 3%) compared to the HURDAT (51.1%), CFSR (56.4%), and JRA-55 (50.4%). FLOR-FA produces better simulations of ET ratio (57.3% ± 3%). The improvement of FLOR-FA relative to FLOR is attributable to improved representations of the large-scale climate conditions (Vecchi et al. 2014). The biases of FLOR in representing large-scale environmental conditions tend to inhibit TC genesis, development, and poleward propagation in the NA (Vecchi et al. 2014).

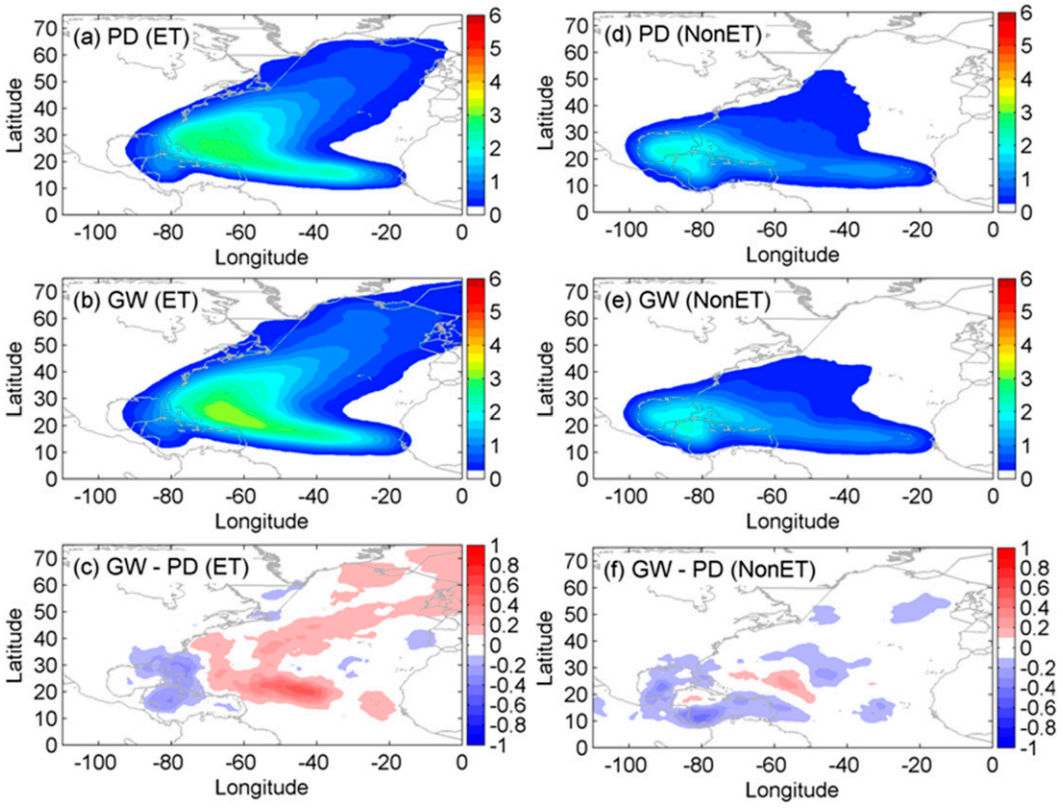

FIG. 15. The annual TC density of ET events in the (a) PD and (b) GW simulations and of non-ET events in the (d) PD and (e) GW simulations.(c),(f) The future change of annual TC density of ET and non-ET events, respectively.

Compared to FLOR-FA, fewer TCs simulated in the standard FLOR model reach the baroclinically active regions indicated by the 700-hPa climatological Eady growth rate.

The FLOR-FA model exhibits good skill in representing the TC density of non-ET and ET events as compared to reanalysis results. The latitude distributions of ET onset and completion are well represented in FLOR-FA. The storm-centered geopotential height composite analyses describe the interactions between TCs and midlatitude baroclinic features, and the results are broadly consistent with previous studies (Klein et al. 2000; Hart et al. 2006; Atallah et al. 2007; Wood and Ritchie 2014).

The FLOR-FA model shows distinct rainfall patterns during the TC and ET/EX stages. During the TC stage, rainfall is organized in a symmetric pattern with the highest rain rate located slightly to the right of storm center. Rainfall in the ET/EX stage is concentrated in the front-left quadrant, relative to the motion of the storm center. These features are broadly consistent with results documented in previous studies (Atallah and Bosart 2003; Jones et al. 2003; Atallah et al. 2007).

The response of ET to the projected twenty-first-century climate change is examined using FLOR-FA through a comparison between a five-member ensemble of present-day (PD) simulations (1961–2005) against global warming (GW) simulations (2056–2100) under the RCP4.5 scenario. We find a slight decrease of annual TC counts and an increase of annual ET counts, but these changes are not statistically significant. The annual ET ratio, however, shows an increase with statistical significance, $p = 0.06$.

The TC density is projected to increase over large areas of the eastern NA but decreases in the western NA, consistent with previous modeling studies (Murakami and Wang 2010; Colbert et al. 2013) and observational estimates over the past 120 years (Vecchi and Knutson 2008). The projected changes of TC genesis appear to be a major cause of the shift of TC tracks (Murakami and Wang 2010).

A decreased density over the western NA is found for both ET and non-ET events. For ET cases, the decrease mainly occurs in the northern Caribbean Sea and the southern United States. For non-ET events, the decrease is located in the southern Caribbean Sea due to

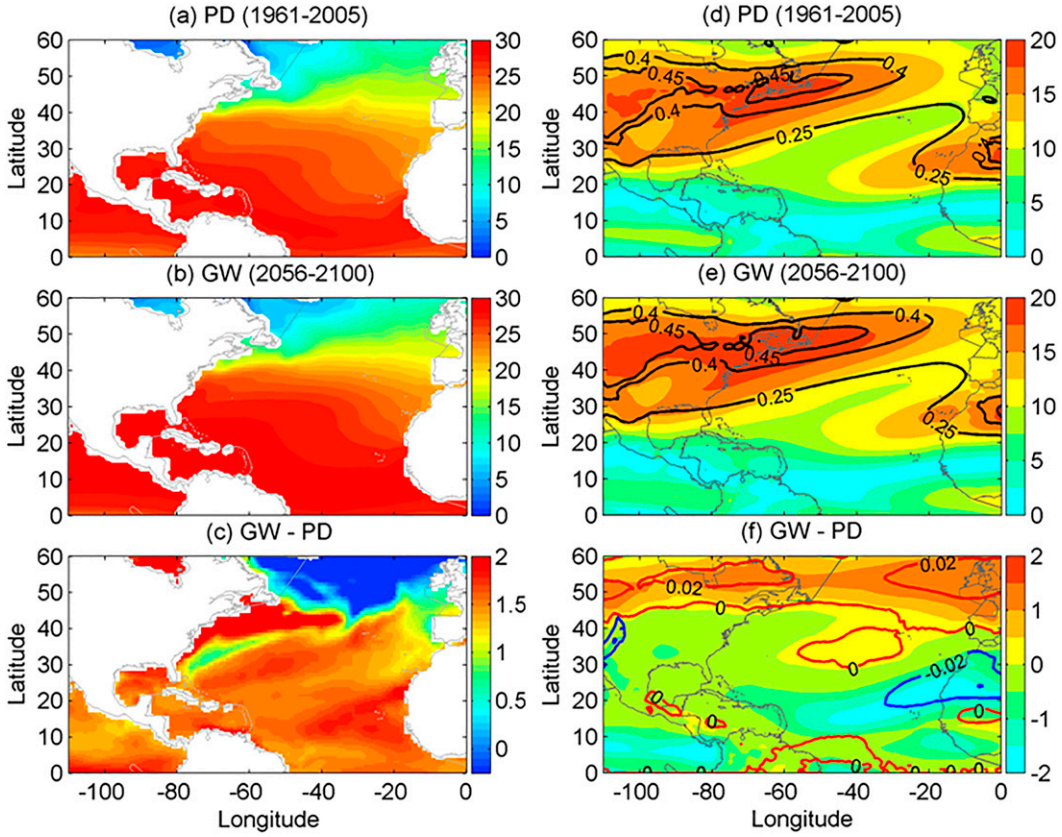

FIG. 16. The climatological monthly sea surface temperature (SST; °C) averaged over July–November in the (a) PD and (b) GW simulations, and (c) the future change. (d)–(f) As in (a)–(c), but for climatological monthly 850–250-hPa wind shear (shaded; m s^{-1}) and Eady growth rate (contour; day^{-1}).

the constraints of northward motion and in the Gulf of Mexico where a relatively high frequency of non-ET cases is observed.

The increased TC density in the eastern NA is mainly from ET events. Specifically, such increases over the eastern tropics of the Atlantic show two paths: one moves northwest toward the northeast coast of the United States, and the other propagates northeast toward western Europe. Future changes in SST and wind shear in these regions highlight an increasingly favorable environment for TC development and propagation. Despite little change of the southern boundary of the baroclinically favorable zone indicated by the Eady growth rate, we hypothesize that TCs are more prone to survive and propagate to midlatitudes in a more favorable environment, and thus are more likely to undergo ET. The dominance of ET events in the increased TC density over the eastern NA is a key element of this hypothesis.

This study was designed to evaluate the utility of high-resolution global climate models to describe the climatology of ET, and also to provide a first step in understanding the potential changes in ET in a warming climate. The ability of FLOR-FA to recover many of the climatological statistics of ET shown in this study provides a basis to explore the seasonal prediction of ET, as has been done for TC activity (e.g., Vecchi et al. 2014). Further, the FLOR-FA provides a solid foundation for future work targeted at a more general

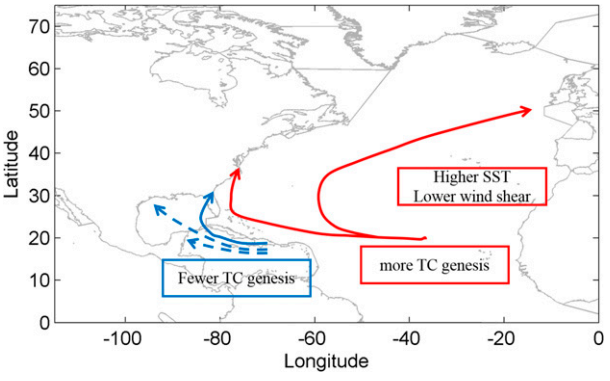

FIG. 17. The schematic map of regional TC density change. The red (blue) arrow denotes increase (decrease) of TC density for typical tracks. The ET (non-ET) event is in solid (dashed) line.

understanding of the dependence of ET climatology on various climate drivers, such as El Niño–Southern Oscillation, the Atlantic multidecadal oscillation, and radiative forcing changes, as well as a better understanding of the impacts of ET. Future studies will examine the climatology of ET in other basins to form a comprehensive understanding of variations, changes, predictability, and impacts of ET.

Acknowledgments. This work was supported in part by Award NA14OAR4830101 from the National Oceanic and Atmospheric Administration, U.S. Department of Commerce, and the National Science Foundation (Grants EAR-1520683 and AGS-1262099). We thank Dr. Dan Li for the very helpful discussion. We thank the two anonymous reviewers for their critical and thoughtful comments, which significantly improved the quality of the paper.

REFERENCES

Agustí-Panareda, A., S. L. Gray, G. C. Craig, and C. Thorncroft, 2005: The extratropical transition of Tropical Cyclone Lili (1996) and its crucial contribution to a moderate extratropical development. *Mon. Wea. Rev.*, **133**, 1562–1573, doi:10.1175/MWR2935.1.

Arnott, J. M., J. L. Evans, and F. Chiaromonte, 2004: Characterization of extratropical transition using cluster analysis. *Mon. Wea. Rev.*, **132**, 2916–2937, doi:10.1175/MWR2836.1.

Atallah, E. H., and L. F. Bosart, 2003: The extratropical transition and precipitation distribution of Hurricane Floyd (1999). *Mon. Wea. Rev.*, **131**, 1063–1081, doi:10.1175/1520-0493(2003)131<1063:TETAPD>2.0.CO;2.

——, ——, and A. R. Aiyyer, 2007: Precipitation distribution associated with landfalling tropical cyclones over the eastern United States. *Mon. Wea. Rev.*, **135**, 2185–2206, doi:10.1175/MWR3382.1.

Baatsen, M., R. J. Haarsma, A. J. Van Delden, and H. de Vries, 2015: Severe autumn storms in future western Europe with a warmer Atlantic Ocean. *Climate Dyn.*, **45**, 949–964, doi:10.1007/s00382-014-2329-8.

Camargo, S. J., 2013: Global and regional aspects of tropical cyclone activity in the CMIP5 models. *J. Climate*, **26**, 9880–9902, doi:10.1175/JCLI-D-12-00549.1.

——, A. W. Robertson, S. J. Gaffney, P. Smyth, and M. Ghil, 2007: Cluster analysis of typhoon tracks. Part I: General properties. *J. Climate*, **20**, 3635–3653, doi:10.1175/JCLI4188.1.

Chavas, D. R., and K. A. Emanuel, 2010: A QuikSCAT climatology of tropical cyclone size. *Geophys. Res. Lett.*, **37**, L18816, doi:10.1029/2010GL044558.

Chen, G., 2011: A comparison of precipitation distribution of two landfalling tropical cyclones during the extratropical transition. *Adv. Atmos. Sci.*, **28**, 1390–1404, doi:10.1007/s00376-011-0148-y.

Chen, J.-H., and S.-J. Lin, 2013: Seasonal predictions of tropical cyclones using a 25-km-resolution general circulation model. *J. Climate*, **26**, 380–398, doi:10.1175/JCLI-D-12-00061.1.

Colbert, A. J., and B. J. Soden, 2012: Climatological variations in North Atlantic tropical cyclone tracks. *J. Climate*, **25**, 657–673, doi:10.1175/JCLI-D-11-00034.1.

——, ——, G. A. Vecchi, and B. P. Kirtman, 2013: The impact of anthropogenic climate change on North Atlantic tropical cyclone tracks. *J. Climate*, **26**, 4088–4095, doi:10.1175/JCLI-D-12-00342.1.

Colle, B. A., 2003: Numerical simulations of the extratropical transition of Floyd (1999): Structural evolution and responsible mechanisms for the heavy rainfall over the northeast United States. *Mon. Wea. Rev.*, **131**, 2905–2926, doi:10.1175/1520-0493(2003)131<2905:NSOTET>2.0.CO;2.

Davis, C. A., S. C. Jones, and M. Riemer, 2008: Hurricane vortex dynamics during Atlantic extratropical transition. *J. Atmos. Sci.*, **65**, 714–736, doi:10.1175/2007JAS2488.1.

Delworth, T. L., and Coauthors, 2006: GFDL's CM2 global coupled climate models. Part I: Formulation and simulation characteristics. *J. Climate*, **19**, 643–674, doi:10.1175/JCLI3629.1.

——, and Coauthors, 2012: Simulated climate and climate change in the GFDL CM2.5 high-resolution coupled climate model. *J. Climate*, **25**, 2755–2781, doi:10.1175/JCLI-D-11-00316.1.

Demirci, O., J. S. Tyo, and E. A. Ritchie, 2007: Spatial and spatiotemporal projection pursuit techniques to predict the extratropical transition of tropical cyclones. *IEEE Trans. Geosci. Remote Sens.*, **45**, 418–425, doi:10.1109/TGRS.2006.882251.

DiMego, G. J., and L. F. Bosart, 1982a: The transformation of Tropical Storm Agnes into an extratropical cyclone. Part I: The observed fields and vertical motion computations. *Mon. Wea. Rev.*, **110**, 385–411, doi:10.1175/1520-0493(1982)110<0385:TTOTSA>2.0.CO;2.

——, and ——, 1982b: The transformation of Tropical Storm Agnes into an extratropical cyclone. Part II: Moisture, vorticity and kinetic energy budgets. *Mon. Wea. Rev.*, **110**, 412–433, doi:10.1175/1520-0493(1982)110<0412:TTOTSA>2.0.CO;2.

Emanuel, K. A., 2013: Downscaling CMIP5 climate models show increased tropical cyclone activity over the 21st century. *Proc. Natl. Acad. Sci. USA*, **110**, 12 219–12 224, doi:10.1073/pnas.1301293110.

Evans, J. L., and R. E. Hart, 2003: Objective indicators of the life cycle evolution of extratropical transition for Atlantic tropical cyclones. *Mon. Wea. Rev.*, **131**, 909–925, doi:10.1175/1520-0493(2003)131<0909:OIOTLC>2.0.CO;2.

Feser, F., M. Schubert-Frisius, H. von Storch, M. Zahn, M. Barcikowska, S. Haeseler, C. Lefebvre, and M. Stendel, 2015: Hurricane Gonzalo and its extratropical transition to a strong European storm. *Bull. Amer. Meteor. Soc.*, **96**, S51–S55, doi:10.1175/BAMS-D-15-00122.1.

Galarneau, T. J., C. A. Davis, and M. A. Shapiro, 2013: Intensification of Hurricane Sandy (2012) through extratropical warm core seclusion. *Mon. Wea. Rev.*, **141**, 4296–4321, doi:10.1175/MWR-D-13-00181.1.

Gnanadesikan, A., and Coauthors, 2006: GFDL's CM2 global coupled climate models. Part II: The baseline ocean simulation. *J. Climate*, **19**, 675–697, doi:10.1175/JCLI3630.1.

Grams, C. M., and S. R. Blumer, 2015: European high-impact weather caused by the downstream response to the extratropical transition of North Atlantic Hurricane Katia (2011). *Geophys. Res. Lett.*, **42**, 8738–8748, doi:10.1002/2015GL066253.

Griffin, K. S., and L. F. Bosart, 2014: The extratropical transition of Tropical Cyclone Edisoana (1990). *Mon. Wea. Rev.*, **142**, 2772–2793, doi:10.1175/MWR-D-13-00282.1.

Haarsma, R. J., W. Hazeleger, C. Severijns, H. de Vries, A. Sterl, R. Bintanja, G. J. van Oldenborgh, and H. W. van den Brink, 2013: More hurricanes to hit western Europe due to global warming. *Geophys. Res. Lett.*, **40**, 1783–1788, doi:10.1002/grl.50360.

Hanley, D., J. Molinari, and D. Keyser, 2001: A composite study of the interactions between tropical cyclones and upper-tropospheric troughs. *Mon. Wea. Rev.*, **129**, 2570–2584, doi:10.1175/1520-0493(2001)129<2570:ACSOTI>2.0.CO;2.

Harr, P. A., and R. L. Elsberry, 2000: Extratropical transition of tropical cyclones over the western North Pacific. Part I: Evolution of structural characteristics during the transition process. *Mon. Wea. Rev.*, **128**, 2613–2633, doi:10.1175/1520-0493(2000)128<2613:ETOTCO>2.0.CO;2.

Harris, L. M., S.-J. Lin, and C. Tu, 2016: High-resolution climate simulations using GFDL HiRAM with a stretched global grid. *J. Climate*, **29**, 4293–4314, doi:10.1175/JCLI-D-15-0389.1.

Hart, R. E., 2003: A cyclone phase space derived from thermal wind and thermal asymmetry. *Mon. Wea. Rev.*, **131**, 585–616, doi:10.1175/1520-0493(2003)131<0585:ACPSDF>2.0.CO;2.

——, and J. L. Evans, 2001: A climatology of the extratropical transition of Atlantic tropical cyclones. *J. Climate*, **14**, 546–564, doi:10.1175/1520-0442(2001)014<0546:ACOTET>2.0.CO;2.

——, ——, and C. Evans, 2006: Synoptic composites of the extratropical transition life cycle of North Atlantic tropical cyclones: Factors determining posttransition evolution. *Mon. Wea. Rev.*, **134**, 553–578, doi:10.1175/MWR3082.1.

Hatsushika, H., J. Tsutsui, M. Fiorino, and K. Onogi, 2006: Impact of wind profile retrievals on the analysis of tropical cyclones in the JRA-25 Reanalysis. *J. Meteor. Soc. Japan*, **84**, 891–905, doi:10.2151/jmsj.84.891.

Hazeleger, W., and Coauthors, 2010: EC-Earth: A seamless Earth-system prediction approach in action. *Bull. Amer. Meteor. Soc.*, **91**, 1357–1363, doi:10.1175/2010BAMS2877.1.

Hoskins, B. J., and P. J. Valdes, 1990: On the existence of storm-tracks. *J. Atmos. Sci.*, **47**, 1854–1864, doi:10.1175/1520-0469(1990)047<1854:OTEOST>2.0.CO;2.

IPCC, 2013: *Climate Change 2013: The Physical Science Basis*. T. F. Stocker et al., Eds., Cambridge University Press, 1535 pp.

Jia, L., and Coauthors, 2015: Improved seasonal prediction of temperature and precipitation over land in a high-resolution GFDL climate model. *J. Climate*, **28**, 2044–2062, doi:10.1175/JCLI-D-14-00112.1.

Jones, S. C., and Coauthors, 2003: The extratropical transition of tropical cyclones: Forecast challenges, current understanding, and future directions. *Wea. Forecasting*, **18**, 1052–1092, doi:10.1175/1520-0434(2003)018<1052:TETOTC>2.0.CO;2.

Kitabatake, N., 2008: Extratropical transition of tropical cyclones in the western North Pacific: Their frontal evolution. *Mon. Wea. Rev.*, **136**, 2066–2090, doi:10.1175/2007MWR1958.1.

——, 2011: Climatology of extratropical transition of tropical cyclones in the western North Pacific defined by using cyclone phase space. *J. Meteor. Soc. Japan*, **89**, 309–325, doi:10.2151/jmsj.2011-402.

Klein, P. M., P. A. Harr, and R. L. Elsberry, 2000: Extratropical transition of western North Pacific tropical cyclones: An overview and conceptual model of the transformation stage. *Wea. Forecasting*, **15**, 373–395, doi:10.1175/1520-0434(2000)015<0373:ETOWNP>2.0.CO;2.

——, ——, and ——, 2002: Extratropical transition of western North Pacific tropical cyclones: Midlatitude and tropical cyclone contributions to reintensification. *Mon. Wea. Rev.*, **130**, 2240–2259, doi:10.1175/1520-0493(2002)130<2240:ETOWNP>2.0.CO;2.

Knutson, T. R., J. J. Sirutis, S. T. Garner, G. A. Vecchi, and I. M. Held, 2008: Simulated reduction in Atlantic hurricane frequency under twenty-first-century warming conditions. *Nat. Geosci.*, **1**, 359–364, doi:10.1038/ngeo202.

——, and Coauthors, 2013: Dynamical downscaling projections of twenty-first-century Atlantic hurricane activity: CMIP3 and CMIP5 model-based scenarios. *J. Climate*, **26**, 6591–6617, doi:10.1175/JCLI-D-12-00539.1.

Kobayashi, S., and Coauthors, 2015: The JRA-55 Reanalysis: General specifications and basic characteristics. *J. Meteor. Soc. Japan*, **93**, 5–48, doi:10.2151/jmsj.2015-001.

Kofron, D. E., E. A. Ritchie, and J. S. Tyo, 2010a: Determination of a consistent time for the extratropical transition of tropical cyclones. Part I: Examination of existing methods for finding "ET time." *Mon. Wea. Rev.*, **138**, 4328–4343, doi:10.1175/2010MWR3180.1.

——, ——, and ——, 2010b: Determination of a consistent time for the extratropical transition of tropical cyclones. Part II: Potential vorticity metrics. *Mon. Wea. Rev.*, **138**, 4344–4361, doi:10.1175/2010MWR3181.1.

Kossin, J. P., S. J. Camargo, and M. Sitkowski, 2010: Climate modulation of North Atlantic hurricane tracks. *J. Climate*, **23**, 3057–3076, doi:10.1175/2010JCLI3497.1.

Krishnamurthy, L., G. A. Vecchi, R. Msadek, A. Wittenberg, T. L. Delworth, and F. Zeng, 2015: The seasonality of the Great Plains low-level jet and ENSO relationship. *J. Climate*, **28**, 4525–4544, doi:10.1175/JCLI-D-14-00590.1.

Leroux, M.-D., M. Plu, D. Barbary, F. Roux, and P. Arbogast, 2013: Dynamical and physical processes leading to tropical cyclone intensification under upper-level trough forcing. *J. Atmos. Sci.*, **70**, 2547–2565, doi:10.1175/JAS-D-12-0293.1.

Liu, M., and J. A. Smith, 2016: Extreme rainfall from landfalling tropical cyclones in the eastern United States: Hurricane Irene (2011). *J. Hydrometeor.*, **17**, 2883–2904, doi:10.1175/JHM-D-16-0072.1.

McAdie, C. J., C. W. Landsea, C. J. Neumann, J. E. David, E. S. Blake, and G. R. Hammer: 2009: Tropical cyclones of the North Atlantic Ocean, 1851–2006 (includes 2007 & 2008 track maps). NCDC, Historical Climatology Series 6-2, 238 pp. [Available online at http://purl.access.gpo.gov/GPO/LPS119129.]

McTaggart-Cowan, R., J. R. Gyakum, and M. K. Yau, 2003: The influence of the downstream state on extratropical transition: Hurricane Earl (1998) case study. *Mon. Wea. Rev.*, **131**, 1910–1929, doi:10.1175//2589.1.

Mokhov, I. I., E. M. Dobryshman, and M. E. Makarova, 2014: Transformation of tropical cyclones into extratropical: The tendencies of 1970–2012. *Doklady Earth Sci.*, **454**, 59–63, doi:10.1134/S1028334X14010127.

Murakami, H., 2014: Tropical cyclones in reanalysis data sets. *Geophys. Res. Lett.*, **41**, 2133–2141, doi:10.1002/2014GL059519.

——, and B. Wang, 2010: Future change of North Atlantic tropical cyclone tracks: Projection by a 20-km-mesh global atmospheric model. *J. Climate*, **23**, 2699–2721, doi:10.1175/2010JCLI3338.1.

——, and Coauthors, 2012: Future changes in tropical cyclone activity projected by the new high-resolution MRI-AGCM. *J. Climate*, **25**, 3237–3260, doi:10.1175/JCLI-D-11-00415.1.

——, B. Wang, T. Li, and A. Kitoh, 2013: Projected increase in tropical cyclones near Hawaii. *Nat. Climate Change*, **3**, 749–754, doi:10.1038/nclimate1890.

——, and Coauthors, 2015: Simulation and prediction of category 4 and 5 hurricanes in the high-resolution GFDL HiFLOR coupled climate model. *J. Climate*, **28**, 9058–9079, doi:10.1175/JCLI-D-15-0216.1.

Ritchie, E. A., and R. L. Elsberry, 2003: Simulations of the extratropical transition of tropical cyclones: Contributions by the midlatitude upper-level trough to reintensification. *Mon. Wea. Rev.*, **131**, 2112–2128, doi:10.1175/1520-0493(2003)131<2112:SOTETO>2.0.CO;2.

Saha, S., and Coauthors, 2010: The NCEP Climate Forecast System Reanalysis. *Bull. Amer. Meteor. Soc.*, **91**, 1015–1057, doi:10.1175/2010BAMS3001.1.

Schenkel, B. A., and R. E. Hart, 2012: An examination of tropical cyclone position, intensity, and intensity life cycle within atmospheric reanalysis datasets. *J. Climate*, **25**, 3453–3475, doi:10.1175/2011JCLI4208.1.

Song, J. J., J. J. Han, and Y. A. Wang, 2011: Cyclone phase space characteristics of the extratropical transitioning tropical cyclones over the western North Pacific. *Acta Meteor. Sin.*, **25**, 78–90, doi:10.1007/s13351-011-0006-y.

Thorncroft, C., and S. C. Jones, 2000: The extratropical transitions of Hurricanes Felix and Iris in 1995. *Mon. Wea. Rev.*, **128**, 947–972, doi:10.1175/1520-0493(2000)128<0947:TETOHF>2.0.CO;2.

Vecchi, G. A., and T. R. Knutson, 2008: On estimates of historical North Atlantic tropical cyclone activity. *J. Climate*, **21**, 3580–3600, doi:10.1175/2008JCLI2178.1.

——, and G. Villarini, 2014: Next season's hurricanes. *Science*, **343**, 618–619, doi:10.1126/science.1247759.

——, K. L. Swanson, and B. J. Soden, 2008: Climate change: Whither hurricane activity? *Science*, **322**, 687–689, doi:10.1126/science.1164396.

——, and Coauthors, 2014: On the seasonal forecasting of regional tropical cyclone activity. *J. Climate*, **27**, 7994–8016, doi:10.1175/JCLI-D-14-00158.1.

Villarini, G., and G. A. Vecchi, 2012: Twenty-first-century projections of North Atlantic tropical storms from CMIP5 models. *Nat. Climate Change*, **2**, 604–607, doi:10.1038/nclimate1530.

——, ——, and J. A. Smith, 2010: Modeling the dependence of tropical storm counts in the North Atlantic basin on climate indices. *Mon. Wea. Rev.*, **138**, 2681–2705, doi:10.1175/2010MWR3315.1.

——, ——, and ——, 2012: U.S. landfalling and North Atlantic hurricanes: Statistical modeling of their frequencies and ratios. *Mon. Wea. Rev.*, **140**, 44–65, doi:10.1175/MWR-D-11-00063.1.

——, D. Lavers, E. Scoccimarro, M. Zhao, M. Wehner, G. Vecchi, T. Knutson, and K. Reed, 2014: Sensitivity of tropical cyclone rainfall to idealized global-scale forcings. *J. Climate*, **27**, 4622–4641, doi:10.1175/JCLI-D-13-00780.1.

Walsh, K. J. E., and Coauthors, 2015: Hurricanes and climate: The U.S. CLIVAR working group on hurricanes. *Bull. Amer. Meteor. Soc.*, **96**, 997–1017, doi:10.1175/BAMS-D-13-00242.1.

Wang, Q., Q. Li, and G. Fu, 2012: Determining the extratropical transition onset and completion times of Typhoons Mindulle (2004) and Yagi (2006) using four methods. *Wea. Forecasting*, **27**, 1394–1412, doi:10.1175/WAF-D-11-00148.1.

Wittenberg, A. T., A. Rosati, N.-C. Lau, and J. J. Ploshay, 2006: GFDL's CM2 global coupled climate models. Part III: Tropical Pacific climate and ENSO. *J. Climate*, **19**, 698–722, doi:10.1175/JCLI3631.1.

Wood, K. M., and E. A. Ritchie, 2014: A 40-year climatology of extratropical transition in the eastern North Pacific. *J. Climate*, **27**, 5999–6015, doi:10.1175/JCLI-D-13-00645.1.

Wright, D. B., T. R. Knutson, and J. A. Smith, 2015: Regional climate model projections of rainfall from U.S. landfalling tropical cyclones. *Climate Dyn.*, **45**, 3365–3379, doi:10.1007/s00382-015-2544-y.

Zhao, M., I. M. Held, S.-J. Lin, and G. A. Vecchi, 2009: Simulations of global hurricane climatology, interannual variability, and response to global warming using a 50-km resolution GCM. *J. Climate*, **22**, 6653–6678, doi:10.1175/2009JCLI3049.1.